

Optical identification of X-ray source 1RXS J180431.1–273932 as a magnetic cataclysmic variable^{*}

N. Masetti¹, A.A. Nucita^{2,3} and P. Parisi^{1,4}

¹ INAF – Istituto di Astrofisica Spaziale e Fisica Cosmica di Bologna, via Gobetti 101, I-40129 Bologna, Italy

² Dipartimento di Matematica e Fisica “Ennio De Giorgi”, Università del Salento, via per Arnesano, I-73100 Lecce, Italy

³ INFN – Istituto Nazionale di Fisica Nucleare, Sezione di Lecce, via per Arnesano, I-73100 Lecce, Italy

⁴ INAF – Istituto di Astrofisica e Planetologia Spaziali, via Fosso del Cavaliere 100, I-00133 Roma, Italy

Received 3 April 2012; accepted 5 July 2012

ABSTRACT

The X-ray source 1RXS J180431.1–273932 has been proposed as a new member of the Symbiotic X-ray Binary (SyXB) class of systems, which are composed of a late-type giant which loses matter to an extremely compact object, most likely a neutron star. In this paper we present an optical campaign of imaging plus spectroscopy on selected candidate counterparts of this object; we also reanalyzed the available archival X-ray data collected with *XMM-Newton*. We found that the brightest optical source inside the 90% X-ray positional error circle is spectroscopically identified as a magnetic cataclysmic variable (CV), most likely of Intermediate Polar type, through the detection of prominent Balmer, He I, He II and Bowen Blend emissions. On either spectroscopic or statistical grounds, we discard as counterparts of the X-ray source the other optical objects in the *XMM-Newton* error circle. A red giant star of spectral type M5 III is found lying just outside the X-ray position: we consider this latter object as a fore-/background one and likewise rule it out as counterpart of 1RXS J180431.1–273932. The description of the X-ray spectrum of the source using a bremsstrahlung plus black-body model gives temperatures $kT_{\text{br}} \sim 40$ keV and $kT_{\text{bb}} \sim 0.1$ keV for these two components. We estimate a distance $d \sim 450$ pc and a 0.2–10 keV X-ray luminosity $L_X \sim 1.7 \times 10^{32}$ erg s^{−1} for this system and, using the information obtained from the X-ray spectral analysis, a mass $M_{\text{WD}} \sim 0.8 M_{\odot}$ for the accreting white dwarf (WD); we also confirm an X-ray periodicity of 494 s from this source which we interpret as the spin period of the WD. In summary, 1RXS J180431.1–273932 is identified as a magnetic CV and its SyXB nature is excluded.

Key words. X-rays: individual: 1RXS J180431.1–273932 — novae, cataclysmic variables — Stars: dwarf novae — Techniques: spectroscopic — Astrometry

1. Introduction

Symbiotic X-ray binaries (SyXBs; see e.g. Masetti et al. 2006a) form a tiny class of low mass X-ray binaries in which the compact accretor, most likely a neutron star (NS), receives matter from a red giant rather than from a late-type companion star on the main sequence (or possibly slightly evolved) and with mass generally $\lesssim 1 M_{\odot}$. These objects are defined SyXBs by analogy with symbiotic binary systems, which are formed by an evolved late-type star and a white dwarf (WD).

Currently there are only 7 confirmed objects of this type known in the Galaxy: 6 cases listed in Masetti et al. (2007), Nespoli et al. (2010) and references therein, to which a newly-identified one, XTE J1743–363, has recently been added (Smith et al. 2012). It is therefore equally important to explore possible new candidates (cf. Masetti et al. 2011) and to spectroscopically confirm the known candidates. Indeed, with respect to the latter issue, Masetti et al. (2012) found by using optical spectroscopy that the SyXB

candidate 2XMM J174016.0–290337 (also known as AX J1740.2–2903) proposed by Farrell et al. (2010) is actually a cataclysmic variable (CV) of dwarf nova type. Likewise, the availability of (sub)arcsec-sized X-ray positions allows one to disentangle possible optical counterpart misidentifications especially in severely crowded fields: this recently occurred in the case of IGR J16393–4643, for which a *Chandra* snapshot (Bodaghee et al. 2012) permitted to pinpoint the correct near-infrared counterpart and to dismiss the one proposed by Nespoli et al. (2010) as a SyXB.

With the aim of confirming (or disproving) the nature of yet another SyXB candidate, we performed an optical imaging and spectroscopic campaign on two possible counterparts of the X-ray source 1RXS J180431.1–273932 (Nucita et al. 2007); we also took this opportunity to reanalyze the X-ray data presented by those authors.

The X-ray object 1RXS J180431.1–273932, first detected in the *ROSAT* bright source survey (Voges et al. 1999), was subsequently observed on October 2005 with *XMM-Newton*. The main results of this observation, reported by Nucita et al. (2007), are: (i) the detection of an X-ray period of 494 s, most likely due to the spin of the compact accretor; (ii) the description of its X-ray spectrum in the 0.2–7 keV range in the form of a power law with index $\Gamma \sim 1$ plus a Gaussian emission at ~ 6.6 keV; and (iii) the

Send offprint requests to: N. Masetti (masetti@iasfbo.inaf.it)

^{*} Partly based on observations collected at the Italian Telescopio Nazionale Galileo, located at the Observatorio del Roque de los Muchachos (Canary Islands, Spain)

detection, with the Optical Monitor (OM) onboard *XMM-Newton*, of an object with magnitude $v \sim 17.2$ at a position consistent with the $\sim 2''$ -radius (1σ , corresponding to $3''.3$ at the 90% confidence level) X-ray error circle of the source.

Concerning the last point, Nucita et al. (2007) found that the OGLE catalogue (Wray et al. 2004) reports a red optical object at $\sim 5''$ from the X-ray position of the source and having a periodicity of about 20.5 days in its *I*-band light curve. On the basis of the optical and near-infrared magnitudes of this object (assuming that the OM and OGLE sources are one and the same), Nucita et al. (2007) concluded that its colors are compatible with those of a red giant star of type M6 III, thus making 1RXS J180431.1–273932 a viable SyXB candidate.

However, the non-negligible (albeit small) displacement between the X-ray and the OGLE objects, together with the lack of optical spectroscopy for the latter, calls for an in-depth investigation of the properties of this source in the optical bands. Besides, the location of the source towards the Galactic centre ($l = 3^\circ 2'$; $b = -2^\circ 9'$) suggests that the field crowdedness might produce source confusion when the positional uncertainty of an object is as large as a few arcsec. We therefore started an optical imaging and spectroscopic campaign to clarify the nature of 1RXS J180431.1–273932 using the Italian Telescopio Nazionale Galileo. We also decided to reanalyze here the *XMM-Newton* data first reported in Nucita et al. (2007) using updated software and response matrices and a more physical model to describe the X-ray spectrum.

The outline of the present paper is as follows: in Sect. 2 we describe our optical and X-ray observations, while Sect. 3 reports the results and Sect. 4 a discussion of them. Finally, in Sect. 5 we summarize our conclusions on this source.

2. Observations

2.1. Optical

All optical data presented here were acquired with the 3.58m Telescopio Nazionale Galileo (TNG), located in La Palma (Canary Islands, Spain) and equipped with the imaging spectrograph DOLORES. This instrument carries a 2048×2048 pixels back-illuminated, thinned E2V 4240 CCD.

2.1.1. Imaging and astrometry

In order to acquire a deeper and better resolution image of the field of 1RXS J180431.1–273932 with respect to the one available from the DSS-II-Red survey¹, on 8 September 2010 we obtained a white-filter snapshot of duration 10 s and start time 20:12:55 UT. In imaging mode, DOLORES can secure a field of $8''.6 \times 8''.6$ with a scale of $0''.252 \text{ pix}^{-1}$.

The image thus acquired was then processed to obtain an astrometric solution based on 30 USNO-A2.0² reference stars in the field of 1RXS J180431.1–273932. The conservative error on the optical position is $0''.252$, which was added in quadrature to the systematic error of the USNO catalogue ($0''.25$ according to Assafin et al. 2001 and Deutsch

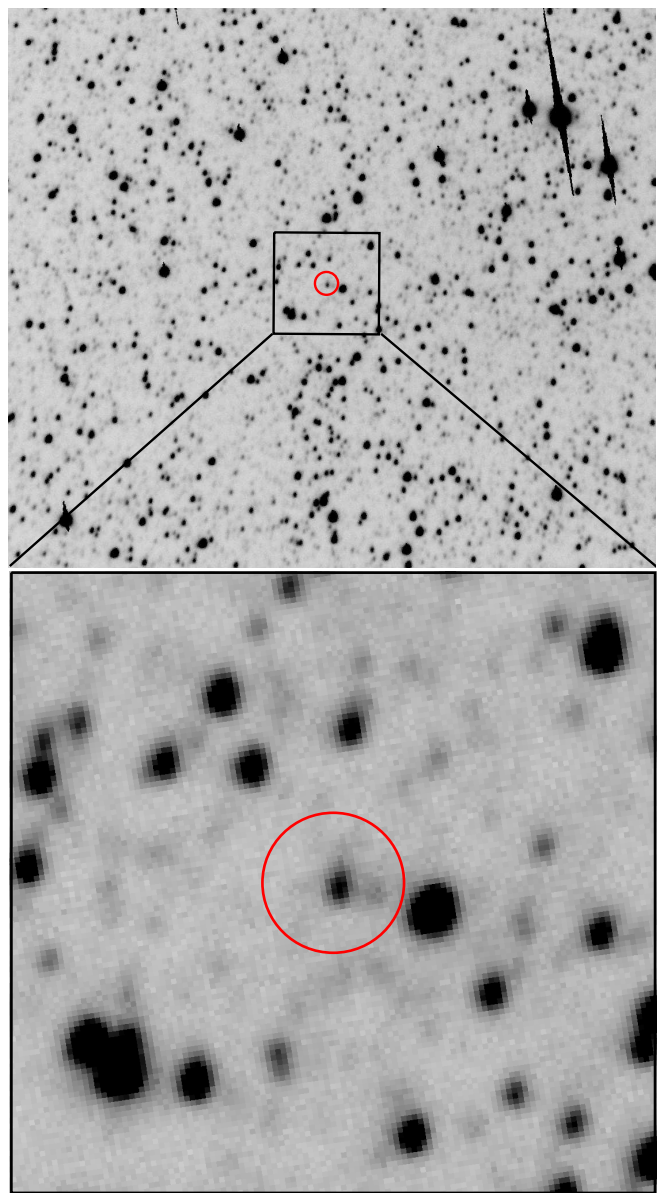


Fig. 1. *Upper panel:* TNG+DOLORES white (open) filter image of the field of 1RXS J180431.1–273932 with superimposed the $3''.3$ -radius 90% confidence level *XMM-Newton* X-ray error circle. The field size is about $3' \times 3'$. *Lower panel:* zoom-in of a $30'' \times 30''$ box centered on the *XMM-Newton* position. The actual counterpart (see text) is the object readily recognizable within the circle; the red giant star mentioned by Nucita et al. (2007) is the bright source just outside the circle on the right. In both panels, North is at top and East is to the left.

1999). The final 1σ uncertainty on the astrometric solution of the image is thus $0''.35$.

Once we determined the astrometry of the image, we superimposed onto it the X-ray error circle determined with the *XMM-Newton* data presented in Nucita et al. (2007; see also Sect. 3). This clearly encircles one relatively bright object (see Fig. 1); a brighter source is also present just outside the *XMM-Newton* error circle, west of it.

To get an estimate of the image depth, we also performed a photometric study of it. Due to the field crowded-

¹ available at <http://archive.eso.org/dss/dss>

² The USNO-A2.0 catalogue is available at <http://archive.eso.org/skycat/servers/usnoa>

ness (see Fig. 1), we chose standard Point Spread Function (PSF) fitting technique by using the DAOPHOT II image data analysis package PSF-fitting algorithm (Stetson 1987) running within MIDAS³.

No absolute calibration in magnitude can be given since this is a white filter frame: however, a 3σ limit of ~ 3 magnitudes fainter than that of the brightest object inside the *XMM-Newton* error circle can be attributed to the depth of the image.

In order to clarify the nature of the two objects mentioned above, and to eventually determine which of the two (if any) is the actual counterpart of the X-ray source, we decided to undertake optical spectroscopy on both.

Additionally, one may note the further presence of fainter objects inside the X-ray error circle (zoom-in of Fig. 1): we will discuss them and exclude their connection with 1RXS J180431.1–273932 in Sect. 3.1.

2.1.2. Spectroscopy

Optical spectroscopic data of the two brightest optical sources mentioned in the previous subsection were acquired on 21 August 2011 using the LR-B grism and a $1''.5$ slit: this setup provided a dispersion of 2.7 \AA/pixel and a nominal wavelength coverage between 3700 and 8100 \AA . The total exposure time was 3×20 min centered at 21:24 UT. The spectrograph slit was suitably oriented in order to acquire the spectra of both objects simultaneously.

The spectra, after correction for flat-field, bias and cosmic-ray rejection, were background subtracted and optimally extracted (Horne 1986) using IRAF⁴. Wavelength calibration was performed using comparison lamps acquired soon after each on-target spectroscopic exposure, while flux calibration was accomplished by observing the spectroscopic standard star Feige 110 (Hamuy et al. 1992, 1994).

Wavelength calibration uncertainty was $\sim 0.5 \text{ \AA}$; this was checked by using the positions of background night sky lines. Spectra from a same object were then stacked together to increase the final signal-to-noise ratio.

2.2. X-rays

As mentioned above, we took this opportunity to reanalyze the X-ray data collected by the *XMM-Newton* satellite towards the source 1RXS J180431.1–273932. The source was observed for $\simeq 100$ ks (Observation ID 30597) with both the EPIC MOS and pn cameras (Strüder et al. 2001; Turner et al. 2001) in thin filter mode. The observation data files (ODFs) were processed using the *XMM-Newton* Science Analysis System (SAS⁵ version 11.0.0) together with the latest calibration constituent files. After processing the raw data via the standard *emchain* and *epchain* tasks, we were left with adequate event lists that were used for the subse-

quent spectral and timing analysis. The J2000 X-ray coordinates of 1RXS J180431.1–273932 were determined once again by using the *edetect_chain* tool on the MOS 1 and MOS 2 images in the 0.3–8.0 keV band. The coordinates in output for the two cameras were then averaged in order to get the best estimate of the target position.

2.2.1. X-ray spectral analysis

For the spectral analysis we further screened the event files by rejecting time intervals affected by high levels of background. These intervals (more evident in the energy range 10–12 keV) were flagged, strictly following the recipe described in the XRPS user's manual⁶, i.e. by selecting a threshold of 0.4 counts s^{-1} and 0.35 counts s^{-1} for the pn and MOS cameras, respectively.

After inspecting by eye that the screening procedure removed effectively the periods of high background activity, the good time intervals resulted in effective exposures of $\simeq 96$ ks, $\simeq 98$ ks, and $\simeq 94$ ks for the MOS 1, MOS 2, and pn cameras, respectively.

The source spectra (one for each EPIC camera) were extracted from a circular region centered on the target position while the background was extracted from source-free circular regions on the same chip and, where possible, at the same vertical location of the source extraction regions. Both the source and background extraction regions had a radius of $64''$. Particular attention had to be paid in the case of the pn camera since the target source is localized on a chip gap. In this case, the background extraction region was chosen on one of the CCDs in a position close to the target and free from other X-ray sources. For the pn data, we decided to accept only single events⁷ (*PATTERN* = 0) while, in the case of the two MOS, all valid patterns (*PATTERN* ≤ 12) were included. In all cases, we also added the selection *FLAG* = 0.

2.2.2. X-ray timing analysis

The timing analysis was performed without applying any selection for good time intervals in order to avoid gaps which could introduce spurious effects. The synchronized source and background light curves were extracted in the 0.3–8 keV energy band for the three EPIC cameras. The light curves were additionally corrected (for absolute and relative corrections, see the XRPS user's manual) by using the *epiclccorr* task and then averaged in order to increase the signal-to-noise ratio. We then searched for periodicity between 5 s and 10 h by using the Lomb-Scargle method (Lomb 1976; Scargle 1982).

3. Results

3.1. Optical

As mentioned in the previous section, our optical imaging shows that a relatively bright object is found within the

³ MIDAS (Munich Image Data Analysis System) is developed, distributed and maintained by the European Southern Observatory and is available at <http://www.eso.org/sci/software/esomidas/>

⁴ IRAF is the Image Analysis and Reduction Facility made available to the astronomical community by the National Optical Astronomy Observatories, which are operated by AURA, Inc., under contract with the U.S. National Science Foundation. It is available at <http://iraf.noao.edu/>

⁵ <http://xmm.esa.int/sas/>

⁶ available at:

http://xmm.esac.esa.int/external/xmm_user_support/documentation/rpsman/index.html

⁷ This was chosen because the energy calibration for single events is slightly better than that for double ones, see e.g. the XRPS user's manual.

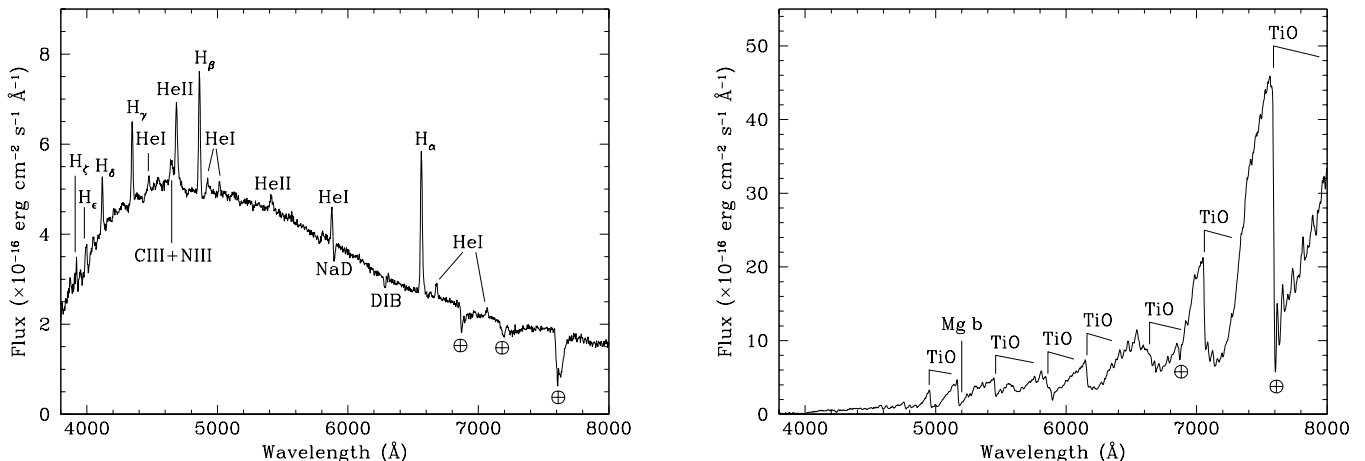


Fig. 2. 3700–8000 Å optical spectra of the two main optical sources mentioned in this paper as possible optical counterparts of the X-ray source 1RXS J180431.1–273932 (see Fig. 1), that is, the most evident of the objects inside the X-ray error circle (left panel) and the bright one just outside it to the west (right panel). The former has a spectrum typical of a magnetic CV, while the latter shows the characteristics of a late-type giant star (see text). In both spectra, the telluric absorption bands are marked with the symbol \oplus .

XMM-Newton error box. This source has coordinates RA = 18^h 04^m 30^s.44, Dec = −27° 39′ 32″.1 (J2000). It lies 0′.9 arcsec from the centre of the X-ray error circle (Nucita et al. 2007; see also Sect. 3.2), thus well within it. A further, brighter source is present slightly outside the X-ray error circle and has coordinates consistent with the OGLE one reported in Nucita et al. (2007). This object is also reported in the 2MASS catalogue (Skrutskie et al. 2006) as 2MASS J18043013–2739340.

The optical spectra of these two objects are reported in Fig. 2. The source inside the X-ray error circle (left panel) shows a number of emission lines, among which we identify the Balmer ones (up to at least H_γ), He I, He II and the Bowen blend around 4640 Å; all features lie at $z = 0$, indicating that this is a Galactic object. Fluxes and EWs of the main emission lines of this object are reported in Table 1.

These spectral characteristics are typical of CVs of dwarf nova type (see e.g. Masetti et al. 2006b); moreover, the Balmer decrement clearly appears negative, the HeII4686/H_β EW ratio is larger than 0.5 and the EWs of He II and H_β are around 10 Å (see Table 1); all this indicates that this source is quite possibly a magnetic CV belonging to the Intermediate Polar (IP) subclass (see Warner 1995 and references therein) not strongly affected by interstellar reddening.

The spectrum of source 2MASS J18043013–2739340 (Fig. 2, right panel) shows instead the typical features of red giants (namely, a series of TiO bands) and no apparent Balmer lines either in emission or in absorption. Using the Bruzual-Persson-Gunn-Stryker (Gunn & Stryker 1983) spectroscopy atlas, we find that the spectrum of the source is strikingly similar to that of star BD −02°3886, of spectral type M5 III. This supports the preliminary classification proposed by Nucita et al. (2007) on the basis of the optical and near-infrared colors of this object.

Unfortunately, the white filter image we acquired does not allow us to determine any reliable optical magnitude for the two objects, due to the breadth of the filter used and the lack of calibration stars for it. We therefore used the

spectral flux information to extract a *V*-band magnitude for both the CV and the red giant. Using the flux-to-magnitude conversion factors of Fukugita et al. (1995) we find $V_{CV} \sim 17.3$ and $V_{RG} \sim 17.5$.

Although the systematic uncertainties tied to this procedure may admittedly be large (possibly up to 20%), we nevertheless are able to give here a broad determination of the optical magnitude of these objects.

These values, assuming absolute magnitudes $M_V \sim +9$ for the CV (Warner 1995) and $M_V \sim +0.7$ (Thé et al. 1990) for a red giant of spectral type M5 III, give the following distances to the two sources: $d_{CV} \sim 450$ pc; $d_{RG} \sim 23$ kpc. We stress that these values (especially the one for the red giant) should conservatively be considered as upper limits, as the effect of the unknown amount of the interstellar absorption along the line of sight was not accounted for in any of the two cases.

As mentioned in the previous section, a few further, fainter objects are present in the *XMM-Newton* X-ray error circle: one lying along the connecting line between the CV and the red giant, and one north of the CV (plus possibly a further, fainter one east of the CV). We can exclude any connection of these optical sources with 1RXS J180431.1–273932 on the basis of the following considerations.

First, due to its sky position, we serendipitously obtained the spectrum of the source located between the CV and the red giant at the same time in which we acquired spectroscopy of these two objects. This is reported in Fig. 3: the presence of the G band at 4304 Å, of the Mg I band at 5175 Å and of the Na I doublet at 5890 Å along with the absence of any peculiar spectral features allow us to classify this source as a star of G type.

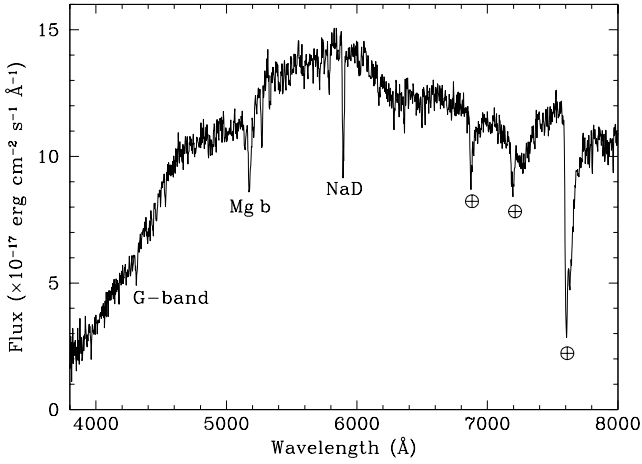
One can note that the optical spectral emission peak of this object lies around 5900 Å, which is more redward than expected in a star of this spectral type (~ 5000 Å; Jaschek & Jaschek 1987): this is most likely due to the blue light being absorbed by interstellar dust along the line of sight. Moreover, this source also shows very weak Ca H+K lines around 4000 Å: although this may appear somewhat

Table 1. List of the main results concerning the CV discovered within the *XMM-Newton* error circle of source 1RXS J180431.1–273932 (see Fig. 1).

H_{α}		H_{β}		$He II \lambda 4686$		V	A_V	d	L_X
EW	Flux	EW	Flux	EW	Flux	mag	(mag)	(pc)	(0.2–10 keV)
20.8 ± 1.0	5.6 ± 0.3	8.9 ± 0.4	4.4 ± 0.2	6.3 ± 0.4	3.0 ± 0.2	~ 17.3	~ 0	~ 450	1.7

Note: EWs are expressed in Å, line fluxes are in units of 10^{-15} erg cm $^{-2}$ s $^{-1}$, whereas the X-ray luminosity observed with *XMM-Newton* is in units of 10^{32} erg s $^{-1}$.

unusual for a G-type star, ‘weak-line’ objects of this kind with abundance anomalies in their chemical composition are known (see e.g. Jaschek & Jaschek 1987); alternatively, these absorptions may be filled up by emission lines connected with the star’s chromospheric activity (Houdebine et al. 2009 and references therein). None of these peculiarities however implies that the observed X-ray emission could be produced by this object.

**Fig. 3.** 3700–8000 Å optical spectrum of the faint object located between the CV and the red giant as seen in the zoom-in of the field of 1RXS J180431.1–273932 (Fig. 1, lower panel). The spectrum is typical of a normal star of G type. Telluric absorption bands are marked with the symbol \oplus .

On the basis of statistical considerations, we next studied the association of the faintest object(s) lying inside the X-ray error box of 1RXS J180431.1–273932 and of brightness ~ 2.5 mag fainter than the CV in our white filter image. From the number density analysis of observed sources in the imaging frame, we expect to randomly find 1.2 objects of such magnitude within an area of the size of the *XMM-Newton* X-ray error circle.

Approaching this issue from a different side, by considering the spatial density of CVs in the Galaxy (Rogel et al. 2008), we find that the probability of finding by chance a CV within 450 pc from Earth in a sky area of size equal to the X-ray error box of this source is less than 6×10^{-7} .

All of the above allows us to say that 1RXS J180431.1–273932 can be identified as a magnetic CV beyond any reasonable doubt.

3.2. X-rays

From the averaged MOS 1 and MOS 2 data in the 0.3–8.0 keV band we found that the X-ray source lies at the position (J2000) RA = 18^h 04^m 30^s.48, Dec = -27° 39′ 32″.76, thus in full agreement with Nucita et al. (2007). The (1σ) statistical uncertainty on the source position, as determined by the *edetect_chain* task, is 0″.05. This value is much smaller than the total 1σ absolute astrometric accuracy of the MOS cameras which was found to be 2″ (see e.g. Kirsch et al. 2004 and Guainazzi 2011⁸). We therefore associate a 90% confidence level error of 3″.3 to both X-ray coordinates of 1RXS J180431.1–273932.

The spectra (binned with at least 25 counts per energy interval) were loaded into the fitting package XSPEC (Arnaud 1996), version 12.0.0.

The data were first fitted with a phenomenological model consisting of an absorbed power law to which a Gaussian line was added. This model was characterized by 6 free parameters (see Nucita et al. 2007 for further details), i.e. the hydrogen column density n_H , the photon index Γ , the line central energy E_L , the emission line width σ_L , the normalization of the Gaussian line N_L and power-law components N_F , respectively.

Then, on the basis of our results of Sect. 3.1, we considered a more physical model built on the basic picture for the accretion onto a magnetized CV (e.g. Mouchet et al. 2008), i.e. absorbed bremsstrahlung and black-body components with a Gaussian line accounting for the emission feature observed at $\simeq 6.6$ keV. A neutral absorber partially covering the source was also used to describe the intrinsic absorption, as sometimes seen in the spectra of similar objects (Rana et al. 2005; Homer et al. 2006).

Practically, the physical model was constituted of 9 free parameters, i.e. the intrinsic hydrogen column density n_H , the covering factor CF , the temperatures of the bremsstrahlung and black-body components (kT_{br} and kT_{bb}) together with their corresponding normalizations (N_{br} and N_{bb}), the Gaussian line central energy E_L , its width σ_L , and the associated normalization N_L . In the physical model, we noted that a stable fit was reached by fixing the neutral hydrogen column density⁹ to the value 0.23×10^{22} cm $^{-2}$.

⁸ See also

http://xmm.esac.esa.int/external/xmm_data_analysis/sas_workshops/sas_ws11_files/

⁹ For comparison, the neutral hydrogen column density in the direction of the target as provided by the “ N_H ” online calculator (<http://heasarc.nasa.gov/cgi-bin/Tools/w3nh/w3nh.pl>) is 0.34×10^{22} cm $^{-2}$ (Kalberla et al. 2005).

Table 2. X-ray spectral fits for 1RXS J180431.1–273932.

Model in XSPEC: phabs*(powerlaw+ gaussian)												
	n_H	Γ	N_Γ (10^{-4})	E_L (keV)	σ_L (keV)	N_L (10^{-4})	χ^2_ν	d.o.f.				
\overline{M}	$0.15^{+0.01}_{-0.01}$	$1.05^{+0.01}_{-0.01}$	$4.0^{+0.1}_{-0.1}$	$6.57^{+0.01}_{-0.01}$	$0.23^{+0.05}_{-0.05}$	$0.17^{+0.04}_{-0.04}$	1.09	396				
$\overline{M,p}$	$0.16^{+0.02}_{-0.02}$	$1.08^{+0.02}_{-0.02}$	$3.8^{+0.1}_{-0.1}$	$6.57^{+0.05}_{-0.05}$	$0.21^{+0.05}_{-0.05}$	$0.16^{+0.03}_{-0.03}$	2.00	575				
$\overline{M,p}$	$0.15^{+0.01}_{-0.01}$	$1.07^{+0.02}_{-0.02}$	$4.0^{+0.1}_{-0.1}$ $3.0^{+0.1}_{-0.1}$	$6.58^{+0.05}_{-0.05}$	$0.23^{+0.04}_{-0.04}$	$0.18^{+0.06}_{-0.06}$ $0.17^{+0.05}_{-0.05}$	1.08	573				
Model in XSPEC: phabs*pcfabs*(bremss + bbodyrad + gaussian)												
	n_H (Phabs)	n_H (Pcfabs)	CF	kT_{br} (keV)	N_{br} (10^{-4})	kT_{bb} (keV)	N_{bb}	E_L (keV)	σ_L (keV)	N_L	χ^2_ν	d.o.f.
\overline{M}	[0.23]	$6.0^{+2.4}_{-2.1}$	$0.28^{+0.07}_{-0.15}$	40^{+50}_{-20}	$12.3^{+4.0}_{-0.7}$	$0.12^{+0.01}_{-0.01}$	217^{+160}_{-100}	$6.59^{+0.07}_{-0.07}$	$0.27^{+0.05}_{-0.05}$	$0.22^{+0.05}_{-0.05}$	1.05	393
$\overline{M,p}$	[0.23]	$5.5^{+2.0}_{-2.0}$	$0.32^{+0.08}_{-0.10}$	30^{+12}_{-8}	$11.01^{+0.05}_{-0.03}$	$0.13^{+0.02}_{-0.02}$	140^{+116}_{-70}	$6.59^{+0.05}_{-0.05}$	$0.26^{+0.05}_{-0.05}$	$0.22^{+0.04}_{-0.04}$	1.93	572
$\overline{M,p}$	[0.23]	$5.6^{+1.5}_{-2.1}$	$0.37^{+0.06}_{-0.10}$	40^{+60}_{-20}	$12.0^{+1.6}_{-0.4}$ $9.0^{+0.7}_{-0.4}$	$0.13^{+0.01}_{-0.01}$	187^{+122}_{-84} 140^{+120}_{-60}	$6.60^{+0.05}_{-0.05}$	$0.27^{+0.05}_{-0.05}$	$0.23^{+0.05}_{-0.05}$ $0.20^{+0.05}_{-0.05}$	1.03	569
Note: When the reduced χ^2_ν is close to the value of 2.0, the errors (90% confidence level) associated to the model parameters were obtained by using the <i>steppar</i> command within XSPEC. Hydrogen columns are in units of 10^{22} cm $^{-2}$. Fixed values in the fits are indicated in square brackets. In the first column, the character M represents the MOS 1 and MOS 2 data sets, and p stands for the pn data. A line over the character (or set of characters) indicates that, in the corresponding fit, the model normalizations were assumed to be identical for the overlined data sets.												

We decided to follow different strategies in fitting the data in order to study in which way (if any) the fact that the source fell on a chip gap of the pn affects the results. In particular, we first fitted each model (either phenomenological or physical) with the same set of parameters to the MOS 1 and MOS 2 data sets only. The results of the best fit procedure correspond to the entries labeled as \overline{M} in Table 2. We then fitted the three EPIC data sets with the same spectral model normalization (see the entries labeled as $\overline{M,p}$). Finally, we fitted again the three data sets simultaneously by requiring a different model normalization of the pn with respect to those of the MOS (which were assumed to be identical). The best fit parameters correspond to those labeled as $\overline{M,p}$ in Table 2.

In correspondence of these entries, we give in Table 2 the component normalizations for both the MOS (first line) and pn (second line), separately.

Note that all the errors of the X-ray fit parameters are quoted at 90% confidence level. When the reduced χ^2_ν is close to the value of 2.0 (as in the case $\overline{M,p}$ for the phenomenological fit) the errors associated with the relevant quantities were computed by using the *steppar* command within XSPEC, by requiring that the χ^2_ν increases by at least 2.71 (Avni 1976).

As one can see from Table 2, the model parameters obtained with the different strategies are equivalent within the errors and, in the case of the phenomenological model, similar to those reported by Nucita et al. (2007). We also note that the pn component normalizations are slightly lower than those of the two MOS, an effect likely due to the fact that the source target is located on a chip gap of the pn camera.

In each case, we estimated the observed flux in the 0.2–10 keV band and the equivalent width (EW) of the line at $\simeq 6.6$ keV. These quantities are given in Table 3, following the same format as above; again, the reported errors are at 90% confidence level.

Table 3. Estimates of the 0.2–10 keV flux and line EW.

Phenomenological model		
	$F_{0.2-10 \text{ keV}}$ (erg s $^{-1}$ cm $^{-2}$)	EW (keV)
\overline{M}	$(5.4^{+0.2}_{-0.3}) \times 10^{-12}$	$0.3^{+0.2}_{-0.2}$
$\overline{M,p}$	$(5.1^{+0.1}_{-0.1}) \times 10^{-12}$	$0.3^{+0.1}_{-0.1}$
$\overline{M,p}$	$(5.4^{+0.2}_{-0.3}) \times 10^{-12}$	$0.3^{+0.2}_{-0.1}$
Physical model		
\overline{M}	$(5.3^{+0.4}_{-0.7}) \times 10^{-12}$	$0.4^{+0.2}_{-0.2}$
$\overline{M,p}$	$(4.8^{+0.2}_{-1.2}) \times 10^{-12}$	$0.5^{+0.3}_{-0.2}$
$\overline{M,p}$	$(5.3^{+0.2}_{-0.9}) \times 10^{-12}$	$0.4^{+0.3}_{-0.2}$

For completeness (and as an example), the spectra and the associated best fits are given in Fig. 4 for the phenomenological (left) and physical model (right), respectively. Here we show the fits corresponding to the case of different normalizations between the MOS and pn cameras ($\overline{M,p}$ case). Red and black data points (and associated solid lines representing the best-fit models) refer to MOS 1 and MOS 2, respectively. The green data points and the superimposed line correspond to the pn.

The results of the spectral analysis imply that the unabsorbed 0.2–10 keV flux of the source is $\simeq 7 \times 10^{-12}$ erg s $^{-1}$ cm $^{-2}$. In the next section we will use the X-ray flux thus obtained together with the estimate of the source distance to get the intrinsic luminosity and, consequently, give a classification of 1RXS J180431.1–273932.

The study of the X-ray light curve allowed us to confirm the existence of the periodic signal at 494.0 s first found by Nucita et al. (2007). We then tested the confidence level of

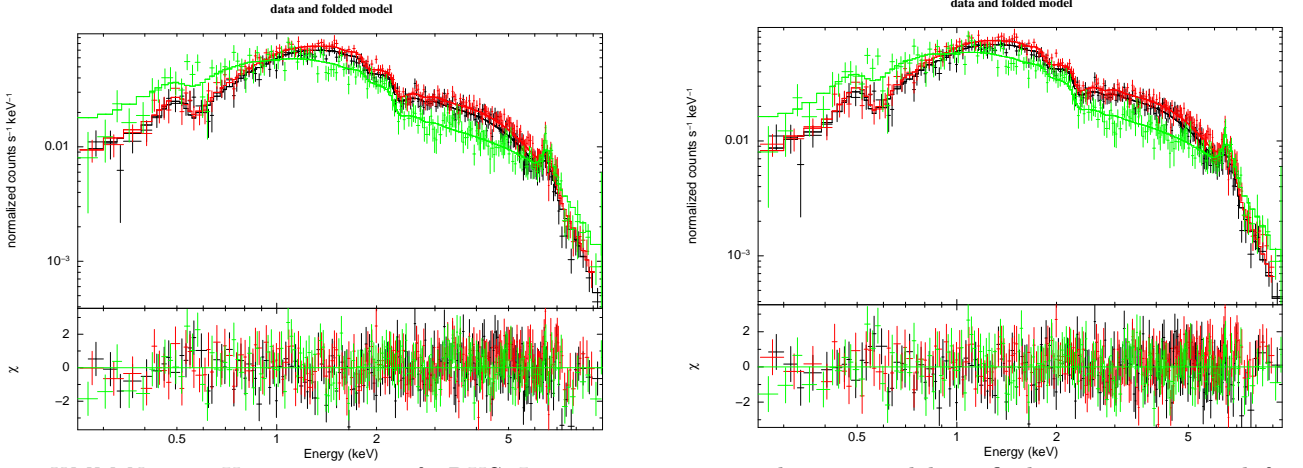


Fig. 4. *XMM-Newton* X-ray spectra of 1RXS J180431.1–273932 and associated best fit lines superimposed for the phenomenological model (left) and the physical model (right). See text for details on the two models. Residuals are reported at the bottom of each panel. Red and black data points refer to MOS 1 and MOS 2, respectively. Green data points are those of the pn.

(The colour version of this figure is available in the on-line journal only)

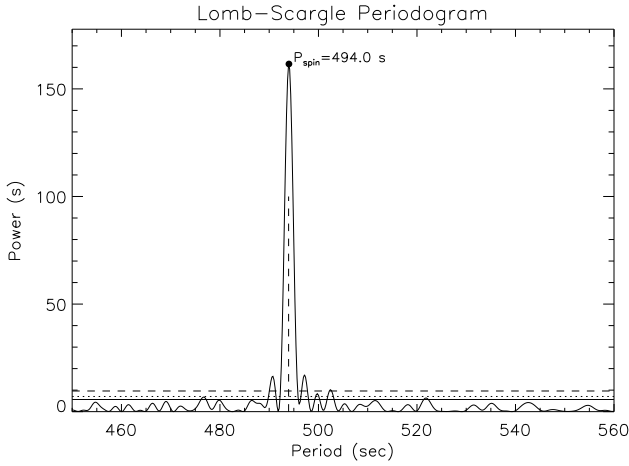


Fig. 5. Lomb-Scargle periodogram of the 0.3–8 keV band light curve of 1RXS J180431.1–273932 with the indication of the detected periodicity. The solid, dotted and dashed horizontal lines represent the 68%, 90% and 99% confidence levels resulted from the Monte Carlo simulations (see text for details).

the detected periodicity by mean of Monte Carlo simulations under the reasonable null hypothesis of white noise. The results of the analysis are shown in Fig. 5 where we give the Lomb-Scargle periodogram. Here, the solid, dotted and dashed horizontal lines represent the 68%, 90% and 99% confidence levels resulted from the Monte Carlo simulations. The error associated with the detected period was estimated by fitting the X-ray light curve with a sine function and keeping the trial periods fixed. By requiring that the chi-square value changes of the quantity $\Delta\chi^2 = 6.63$ (see e.g. Carpano et al. 2007), we found the 3σ error of the 494.0 s pulse period to be 0.1 s. Note that the detected periodicity may be associated with the spin of a compact accretor, most likely a WD (see Sect. 4 for further details on this conclusion).

In Fig. 6, we give the total (MOS+pn) 0.3–8 keV band light curve folded at the detected period and with 20 bins.

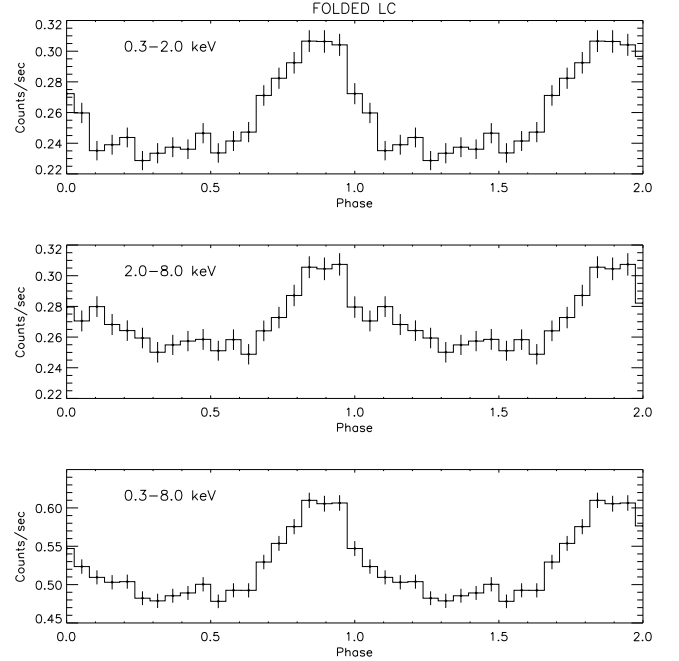


Fig. 6. Total (MOS+pn) 0.3–8 keV band light curve folded at 494.0 s using 20 bins (see text for details).

The zero phase is associated with the beginning of the *XMM-Newton* observation.

The light curve was then binned at twice the detected periodicity (see Fig. 7) in order to search for a variability in the X-ray signal. By fitting the light curve with a simple linear function, we found a clear trend in the data (as already noted in Nucita et al. 2007) corresponding to a decrease in the count rate of $\sim 10^{-4}$ counts s $^{-1}$ hr $^{-1}$, and a variability on the time scale of hours.

4. Discussion

Using optical imaging and spectroscopy we investigated two sources in the X-ray error circle of 1RXS

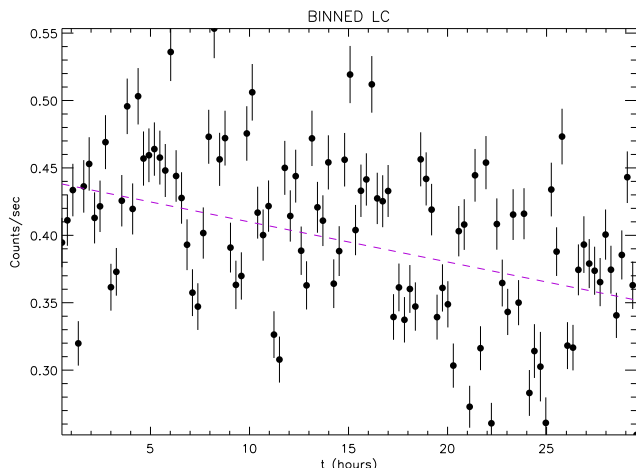


Fig. 7. MOS+pn 0.3–8 keV light curve binned at twice the 494.0 s periodicity (see text for details) together with the best linear fit superimposed (dashed line).

J180431.1–273932 and in its proximity. We found that the one lying within the circle is a magnetic CV, while the other, slightly outside the error box, is a red giant as correctly inferred by Nucita et al. (2007).

This latter fact led those authors to put forward the possibility that this X-ray source could be a new member of the small class of SyXBs; however, the presence of a magnetic CV within the error circle and the positional displacement between the red giant and the X-ray position led us to conclude that the actual X-ray emitter is the CV.

Magnetic CVs are known to be X-ray sources; in particular, in recent years, thanks to the *INTEGRAL* and *Swift* missions many of them were discovered or detected at energies above 20 keV (Barlow et al. 2006; Brunschweiler et al. 2009; Landi et al. 2009; Scaringi et al. 2010); moreover, the spin period range of the WD hosted in these systems, in particular the ones in IPs (see e.g. Butters et al. 2011) encompasses the 494 s X-ray periodicity detected by Nucita et al. (2007) from 1RXS J180431.1–273932, which can thus be interpreted as such. Also, the presence of an iron emission line around 6.6 keV with an EW of several hundreds of eV is a typical X-ray spectral characteristic of magnetic CVs (de Martino et al. 2008). In the same vein, we see that the 0.2–10 keV band softness ratio (as defined in Ramsay & Cropper 2004) computed using the unabsorbed fluxes of the black-body ($\sim 5.5 \times 10^{-13}$ erg cm $^{-2}$ s $^{-1}$) and thermal bremsstrahlung ($\sim 6.5 \times 10^{-12}$ erg cm $^{-2}$ s $^{-1}$) components is in the present case ~ 0.02 , a value typical of IP systems (Evans & Hellier 2007). To all this one can add that the bremsstrahlung temperature and the 0.2–10 keV luminosity of the source (which is 1.7×10^{32} erg s $^{-1}$ assuming the distance determined in the previous section) are comparable with those typical of these sources (as can be determined from, e.g., Landi et al. 2009). All this supports the identification of this X-ray source as a magnetic CV.

We stress that it is known (see e.g. Masetti et al. 2006a, 2007) that the optical spectra of red giant companions in SyXBs do not generally show any peculiarity such as emission lines (the only notable exception being GX 1+4: Chakrabarty & Roche 1997), so on this basis the object 2MASS J18043013–2739340 cannot be ruled out as the optical counterpart of 1RXS J180431.1–273932. However, the fact that (i) it lies nominally outside the X-ray error cir-

cle of this high-energy source, and (ii) a magnetic CV is actually found inside this circle makes us confidently state that this X-ray source is not a SyXB, but rather a magnetic CV, likely of IP type, and that the red giant is just a fore-/background object.

To conclude, we can use some of the results from the physical description of the X-ray spectrum to infer parameters relative to the X-ray emitter. In particular, using the bremsstrahlung component temperature ($kT_{\text{br}} \sim 40$ keV) and Eq. (3) of Middleton et al. (2012), we obtain a mass $M_{\text{WD}} = 0.8^{+0.4}_{-0.3} M_{\odot}$ for the accreting WD hosted in this system (the quoted errors are at 90% confidence level). This, considering the X-ray luminosity of the source and assuming a radius $R_{\text{WD}} \sim 6700$ km for a WD with mass $0.8 M_{\odot}$ (Nauenberg 1972), implies an average mass accretion rate $\dot{m} \sim 1.6 \times 10^{-11} M_{\odot} \text{ yr}^{-1}$ for the source. Likewise, from the best-fit value of the black-body normalization we determine a radius $r_{\text{bb}} \sim 1$ km for the area of this emission component. This value is quite modest when compared with the size of the WD surface; however, it is not uncommon in magnetic CVs (see e.g. Anzolin et al. 2008).

Again following Anzolin et al. (2008), and considering the presence around the WD of an accretion disk truncated at the magnetospheric radius r_{mag} , we can assume that this quantity is comparable in size with the corotation radius r_{co} , which is the radius at which the magnetic field of the WD rotates with the same Keplerian frequency of the inner edge of the accretion disk. In this hypothesis, we can determine the magnetic moment of the WD hosted in 1RXS J180431.1–273932 to be $\mu \sim 3.7 \times 10^{32}$ G cm 3 .

5. Conclusions

Our multiwavelength optical/X-ray study of 1RXS J180431.1–273932 allowed us to identify its actual counterpart and to pinpoint its real nature. We found that this object is a magnetic CV, most likely of IP type; the SyXB hypothesis, put forward by Nucita et al. (2007), is thus ruled out. This misidentification was likely induced by the presence of a red giant along the line of sight and lying just outside the border of the X-ray error box. We also exclude any connection of the X-ray source with other, fainter optical objects within its positional uncertainty obtained from *XMM-Newton* data.

We confirm the X-ray periodicity of 494 s first detected by Nucita et al. (2007) and interpret it as the spin period of the accreting WD hosted in this system. We could also successfully model the X-ray spectrum of 1RXS J180431.1–273932 using a bremsstrahlung plus black-body emission model, as typically found in magnetic CVs. We encourage follow-up observations in optical and X-rays to determine the orbital period and the main physical characteristics of this CV, also in order to confirm the IP nature proposed here.

This research moreover stresses that it is of paramount importance to have very precise (better than a few arcsec) X-ray localizations, especially in cases of crowded fields and particularly for these objects which are concentrated towards the Galactic bulge, in order to determine the optical counterpart.

Acknowledgements. We thank Aldo Fiorenzano for the Service Mode optical observations acquired at TNG and presented in this paper, and Domitilla de Martino for suggestions. AAN is grateful to Stefania

Carpano for interesting discussions. We also thank the anonymous referee for useful remarks which helped us to improve the quality of this paper. This research has made use of the NASA Astrophysics Data System Abstract Service and the NASA/IPAC Infrared Science Archive, which are operated by the Jet Propulsion Laboratory, California Institute of Technology, under contract with the National Aeronautics and Space Administration. This publication made use of data products from the Two Micron All Sky Survey (2MASS), which is a joint project of the University of Massachusetts and the Infrared Processing and Analysis Center/California Institute of Technology, funded by the National Aeronautics and Space Administration and the National Science Foundation. This paper is also based on observations from *XMM-Newton*, an ESA science mission with instruments and contributions directly funded by ESA Member States and NASA. NM acknowledges financial contribution from the ASI-INAF agreement No. I/009/10/0.

References

- Anzolin, G., de Martino, D., Bonnet-Bidaud, J.-M., et al. 2008, *A&A*, 489, 1243
- Arnaud, K.A. 1996, *XSPEC: The First Ten Years*, in *Astronomical Data Analysis Software and Systems V*, ed. G. Jacoby, & J. Barnes, ASP Conf. Ser., 101, 17 (San Francisco: ASP)
- Assafin, M., Andrei, A.H., Vieira Martins, R., et al. 2001, *ApJ*, 552, 380
- Avni, Y. 1976, *ApJ*, 210, 642
- Barlow, E.J., Knigge, C., Bird A.J., et al. 2006, *MNRAS*, 372, 224
- Bodaghee, A., Rahoui, F., Tomsick, J.A., & Rodriguez, J. 2012, *ApJ*, 751, 113
- Brunschweiler J., Greiner J., Ajello M., et al. 2009, *A&A*, 496, 121
- Butters, O.W., Norton, A.J., Mukai, K., & Tomsick, J.A. 2011, *A&A*, 526, A77
- Carpano, S., Pollock, A.M.T., Prestwich, A., et al. 2007, *A&A*, 466, 17
- Chakrabarty, D., & Roche, P. 1997, *ApJ*, 489, 254
- de Martino, D., Matt, G., Mukai, K., et al. 2008, *Mem. Soc. Astron. Ital.*, 79, 246
- Deutsch, E.W. 1999, *AJ*, 118, 1882
- Evans, P.A., & Hellier, C. 2007, *ApJ*, 663, 1277
- Farrell, S.A., Gosling, A.J., Webb, N.A., et al. 2010, *A&A*, 523, A50
- Fukugita, M., Shimasaku, K., & Ichikawa, T. 1995, *PASP*, 107, 945
- Guainazzi, M. 2011, *XMM-SOC-CAL-TN-0018*, *XMM-Newton Science Operations Centre*, <http://xmm.vilspa.esa.es/docs/documents/CAL-TN-0018.pdf>
- Gunn, J.E., & Stryker, L.L. 1983, *ApJS*, 52, 121
- Hamuy, M., Walker, A.R., Suntzeff, N.B., et al. 1992, *PASP*, 104, 533
- Hamuy, M., Suntzeff, N.B., Heathcote, S.R., et al. 1994, *PASP*, 106, 566
- Horne, K. 1986, *PASP*, 98, 609
- Homer, L., Szkody, P., Henden, A.A., et al. 2006, *AJ*, 132, 2743
- Houdebine, E.R., Junghans, K., Heanue, M.C., & Andrews, A.D. 2009, *A&A*, 503, 929
- Jaschek, C., & Jaschek, M. 1987, *The Classification of Stars* (Cambridge: Cambridge Univ. Press)
- Kalberla, P.M.W., Burton, W.B., Hartmann, D., et al. 2005, *A&A*, 440, 775
- Kirsch, M.G.F., Altieri, B., Chen, B., et al. 2004, *Proc. SPIE*, 5488, 103
- Landi, R., Bassani, L., Dean, A.J., et al. 2009, *MNRAS*, 392, 630
- Lomb, N.R. 1976, *Ap. Space Sci.*, 39, 447
- Masetti, N., Orlandini, M., Palazzi, E., Amati, L., & Frontera, F. 2006a, *A&A*, 453, 295
- Masetti, N., Morelli, L., Palazzi, E., et al. 2006b, *A&A*, 459, 21
- Masetti, N., Landi, R., Pretorius, M.L., et al. 2007, *A&A*, 470, 331
- Masetti, N., Munari, U., Henden, A.A., et al. 2011, *A&A*, 534, A89
- Masetti, N., Parisi, P., Jiménez-Bailón, E., et al. 2012, *A&A*, 538, A123
- Middleton, M.J., Cackett, E.M., Shaw, C., et al. 2012, *MNRAS*, 419, 336
- Mouchet, M., Bonnet-Bidaud, J.M., & de Martino, D. 2008, *Mem. Soc. Astron. Ital.*, 75, 282
- Nauenberg, M. 1972, *ApJ*, 175, 417
- Nespoli, E., Fabregat, J., & Mennickent, R.E. 2010, *A&A*, 516, A94
- Nucita, A.A., Carpano, S., & Guainazzi, M. 2007, *A&A*, 474, L1
- Ramsay, G., & Cropper, M. 2004, *MNRAS*, 347, 497
- Rana, V.R., Singh, K.P., Barrett, P.E., & Buckley, D.A.H. 2005, *ApJ*, 625, 351
- Rogel, A.B., Cohn, H.N., & Lugger, P.M. 2008, *ApJ*, 675, 373
- Scargle, J.D. 1982, *ApJ*, 263, 385
- Scaringi, S., Bird, A.J., Norton, A.J., et al. 2010, *MNRAS*, 401, 2207
- Skrutskie, M.F., Cutri, R.M., Stiening, R., et al. 2006, *AJ*, 131, 1163
- Smith, D.M., Markwardt, C.B., Swank, J.H., & Negueruela, I. 2012, *MNRAS*, 422, 2661
- Stetson, P.B. 1987, *PASP*, 99, 191
- Strüder, L., Briel, U., Dennerl, K., et al. 2001, *A&A*, 365, L18
- Thé, P.S., Thomas, D., Christensen, C.G., Westerlund, B.E. 1990, *PASP*, 102, 565
- Turner, M.J.L., Abbey, A., Arnaud, M., et al. 2001, *A&A*, 365, L27
- Voges, W., Aschenbach, B., Boller, T., et al. 1999, *A&A*, 349, 389
- Warner, B. 1995, *Cataclysmic variable stars* (Cambridge: Cambridge University Press)
- Wray, J.J., Eyer, L., & Paczyński, B. 2004, *MNRAS*, 349, 1059